NUMERICAL TRANSIENT HEAT TRANSFER ANALYSIS OF MULTI LASER TRACK ON POWDER BED OF NI-BASED ALLOY

T.-T. Ikeshoji*, H. Kyogoku†, M. Yonehara*, M. Araki**, K. Nakamura**

*Research Institute of Fundamental Technology for Next Generation, Kindai University, 1 Takaya Umenobe, Higashi Hiroshima, Hiroshima, 739-2116, Japan
†Department of Robotics, Kindai University, 1 Takaya Umenobe, Higashi Hiroshima, Hiroshima, 739-2116, Japan
**Technology Research Association for Future Additive Manufacturing, 1-2-19, Nihonbashi, Chuo-ku, Tokyo, 103-0027, Japan

Abstract

The numerical transient heat transfer analysis is conducted for SLM process of Ni-based alloy. For the initial situation, the powder layer covers all the top surface of bulk substrate. Then it is simulated a laser spot scans one and half times of round trips. To simulate the melting of powder layer and its solidification, the powder elements are changed to the bulk when the powder element's temperature reaches to liquidus. The results show the change in melt pool shape. It is symmetry about scanning direction axis for the first path, but the second and third paths' melt pool is wider on the solidified side. The melt pool dimensions are compared with the experimentally obtained thermography images. The estimated melt pool depth is also compared with the metallographic microstructure image of cross section. The results might suggest the one-path simulation is not enough for the prediction of solidified track of SLM process.

Introduction

The selective laser melting (SLM) is the process to melt the thin powder bed by laser scanning. The major factors of the building conditions are the laser power p W, the laser spot size Ø d mm, the scanning speed v mm/s, the laser hatching width w mm, and the layer thickness t mm. The four factors of them can be summarized into the energy density, $E=p/(v \times w \times t)$ J/mm³. For the first idea, the suitable condition will be adjusted to make this energy density equal to the volumetric enthalpy of powder at its liquidus temperature, or melting point, H J/mm³. But, usually the suitable energy density value is much higher than the value of H. Because the physical phenomena other than the melting are involved in the SLM process. For example, the

thermal diffusion, evaporation of melt metal, spattering, and so on. Then it is still necessary to search the suitable energy density value by experimental trials and errors. Therefore, the numerical simulations to help in the searching of proper conditions is expected to develop.

In this research, to develop the numerical simulation technique with high accuracy and reasonably short time, the transient heat transfer analysis was conducted for the selective laser melting process. The melt pool length is estimated by numerical simulation. To check the accuracy of the simulation, the temperature distribution around melt pool on powder bed is measured by thermoviewer, and the length of melt pool was obtained experimentally. The experimentally obtained melt pool length and the numerically estimated values are compared.

Thermographic Measurement of Powder Bed Surface

In Fig.1 (a), the set-up of the temperature distribution measurement on the power bed is shown. The thermoviewer was inserted from the left side of the building chamber with the angle of $40°$ to the vertical line. The lighting is shown in the image but it was not lit during the measurement. On the stage, the base metal of soft steel was amounted. The base plated was set to keep $50°$ C. On the base metal, the powder of Inconel 718 was coated by the recoater. The average diameter of the powder was Ø42 μm. The temperature measurement was conducted after more than 10 times of recoating of powder and laser abrasion. Because of these laser abrasion, the fresh recoated powder bed temperature was higher than the base plate temperature in setting.

The conditions of the selective laser melting process was the laser power p = 292 W, laser spot diameter d = Ø0.1 mm, the scanning speed v = 610 mm/s, the hating pitch w = 0.15 mm and the layer thickness t = 0.05 mm. The laser was scanned in the serpent style whose width was 5 mm.

In Fig.1(b), the typical temperature distribution image, or thermograph around the melt pool is shown. The melt pool was considered the region above the liquidus of Inconel718, *i.e.* $1340°$ C. The shape of the melt pool was not in the symmetrical tear drop shape. The powder region side was relatively flat compared with the solidified region.

The length of the melt pool was defined as the length from the top of the melt pool to its tail tip. From a line of laser scan, which began from the folding back point to another folding back point of serpent style scanning path, 7 thermograph image in equal interval were obtained and the melt pool length was measured for each image(Fig.2). The #1 image was neglected because it was the image for the folding back point and the melt pool did not fully grow. The average of melt pool

length was 1.06 mm.

Transient Heat Transfer Analysis for SLM Process

The transient heat transfer analysis is conducted for the calculated region shown in Fig.3. The scanning length is 5 mm and 10 times scan was simulated. The building conditions were p = 292 W, d = 0.1 mm, v = 610 mm/s, w = 0.15 mm, t = 0.05 mm. The initial temperature of powder and bulk plate was set to 323 K (50º C). The laser power distribution was assumed to Gaussian distribution. On the side and bottom surfaces, it was applied the heat conduction condition of 20 W/(K· m) and the temperature outside of those surfaces was set to 323 K (50º C).

Thermal Properties of Inconel 718 bulk and powder is described as follows. According to the

(a) (b)
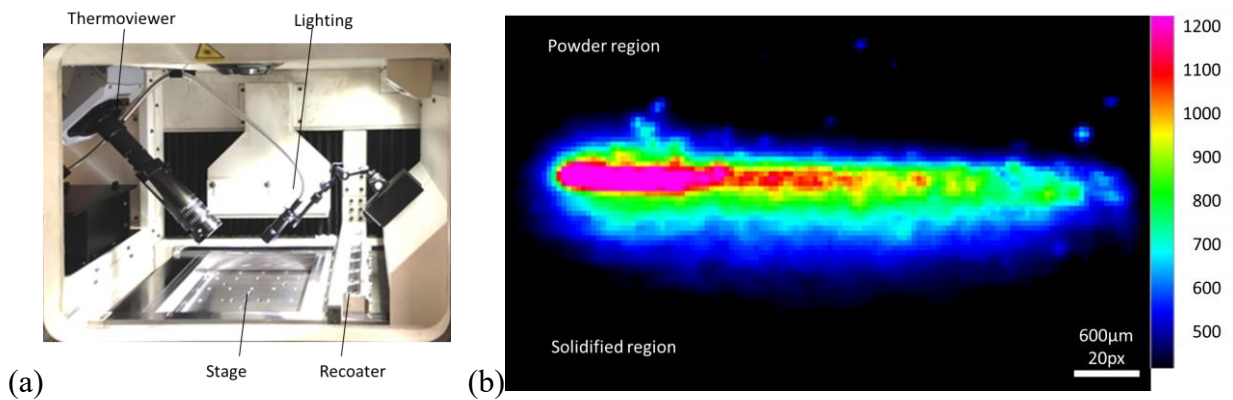
Fig.1 Measurement of temperature distribution around melt pool on powder bed. (a) Apparatus. (b) Thermograph around melt pool.
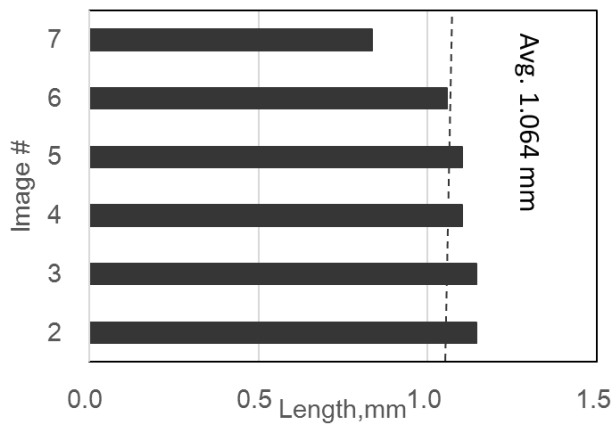
Fig.2 Measured melt pl length.

density ρ^b kg/m³ and specific enthalpy h_m^B J/kg measured experimentally[1,2].

$$h_m^b(T) = \begin{cases} -104{,}989 + 286T + 0.165T^2 & \\ & (400 < T < 1000 \ \text{K}) \\ -319{,}284 + 652T & (1000 < T < 1528 \ \text{K}) \\ -4.7596 \times 10^6 + 3.5580 \times 10^3 T & \\ & (1528 < T < 1610 \ \text{K}) \\ -283{,}854 + 778T & (1610 < T < 2100 \ \text{K}) \end{cases}$$

$$\rho^b(T) = \begin{cases} 8256.42 - 0.2019T - 1.3779 \times 10^{-4}T^2 & \\ & (400 < T < 1000 \ \text{K}) \\ 8392 - 0.431T & (1000 < T < 1528 \ \text{K}) \\ 1.0587 \times 10^4 - 1.8672T & \\ & (1528 < T < 1610 \ \text{K}) \\ 8366 - 0.488T & (1610 < T < 2100 \ \text{K}) \end{cases}$$

c^b, J/(kg K)

$$c^b(T) = \frac{dh_m^b}{dT} = \begin{cases} 286 + 0.3370T & (400 < T < 1000 \ \text{K}) \\ 652 & (1000 < T < 1528 \ \text{K}) \\ 778 & (1610 < T < 2100 \ \text{K}) \end{cases}$$

The volumetric specific enthalpy H_v J/m³ was evaluated as follows,

$$H_v^b(T) = \int_{T_0}^{T} \rho^b c^b \, dT$$

$$H_v^b = \begin{cases} -1.1600 \times 10^9 + 2.3613 \times 10^6 \ T + 1.3623 \times 10^3 \ T^2 & \\ \quad -3.5435 \times 10^{-2} \ T^3 - 1.1272 \times 10^{-5} & 400 < T < 1000 \ \text{K} \\ -2.8141 \times 10^9 + 5.4716 \times 10^6 T - 1.4051 \times 10^2 T^2 & 1000 < T < 1528 \ \text{K} \\ -4.4581 \times 10^{10} + 3.76667 \times 10^7 T - 3321.76T^2 & 1528 < T < 1610 \ \text{K} \\ -2.5345 \times 10^9 + 6.5088 \times 10^6 T - 1.8983 \times 10^2 T^2 & 1610 < T < 2100 \ \text{K} \end{cases}$$

The heat conductivity λ W/(K· m) is

$$\lambda = \begin{cases} 1.1224 + 0.0165T & T < 1528 \ \text{K} \\ 4.8985 + 0.0136T & 1600 < T < 2100 \ \text{K} \end{cases}$$

Estimated values were used for material properties of Inconel 718 powder. The powder density ρ^p kg/m³ was estimated using the bulk density ρ^b and void ratio of powder ϵ.

$$\rho^p(T) = (1 - \epsilon)\rho^b(T)$$

The volumetric specific enthalpy of powder H_v^P J/m³ was decided in similar manner.

$$H_v^P(T) = (1 - \epsilon)H_v^b(T)$$

The heat conductivity of powder is estimated using Kunii-Smith model[3].

$$\lambda^P(T) = \left\{ \epsilon\left(1 + \beta\frac{h_{rv}D_p}{k_g}\right) + \frac{\beta(1-\epsilon)}{\left(\frac{1}{\phi} + \frac{h_{rs}D_p}{\lambda^g}\right)^{-1} + \gamma\left(\frac{\lambda^g}{\lambda^b}\right)} \right\} \lambda^g$$

Profiles of these thermal properties is shown in Fig.4

To simulate the melting and solidification of powder, finite elements' material properties were changed by their temperature values. For a finite element with powder material property, when its temperature value raised up to the liquidus of Inconel 718, *i.e.* 1610 K, its material property of enthalpy and thermal conductivity changed from the property for powder to for bulk. The
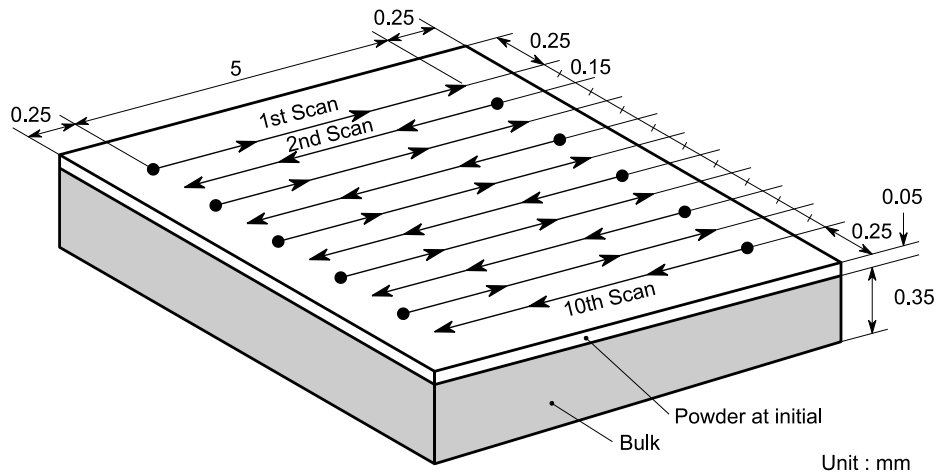
Fig.3 The calculated region.
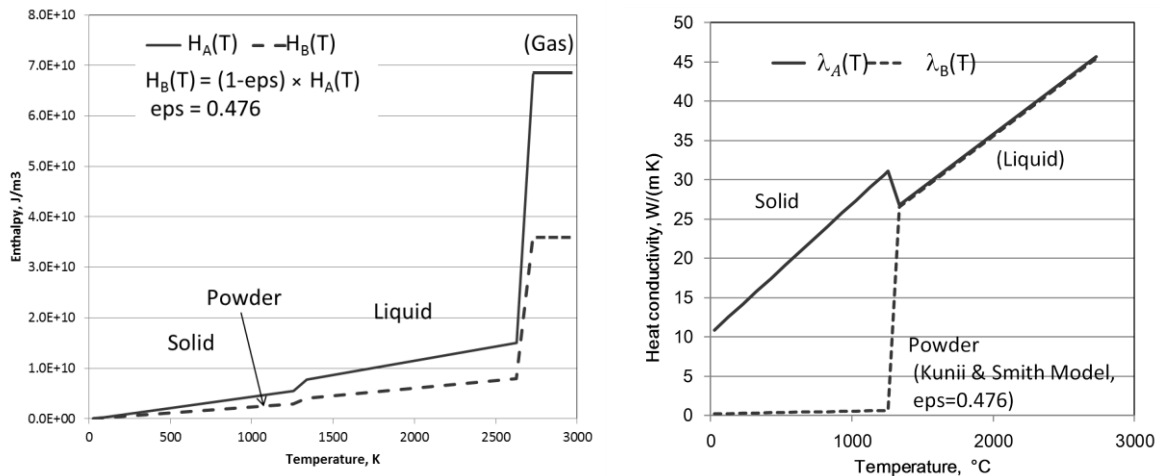
Fig.4 Material properties of Inconel 718 bulk and powder.

enthalpy value was multiplied by $1 - \epsilon$. Because the net amount of powder inside a finite element volume was lower by vacant ratio than that of bulk.

The laser power was applied to the top surface of the calculated region in the form of heat flux. The laser power distribution was assumed Gaussian profile. The absorption rate was fixed to 0.15. This value is derived from the emissivity value set to the thermoviewer. According the Kirchhoff's law, the absorption rate equals to the thermal radiation rate, *i.e.* the emissivity.

Results

Figure 6 shows the change in melt pool sizes with calculation time. At 4.1 ms after the onset of calculation, the melt pool length was 0.85 mm and its width was 0.22 mm. The length of melt pool was long during the first scanning path, then it decreased to 0.74 mm and became almost steady value. Its value, however, gradually increase with the number of scanning path. The width of melt pool was largest during the first scanning path, and became the similar value after the second scanning path. The depth was smallest during the first scanning path, and slightly increased after the second scanning path. Its values were almost same with the number of the scanning path.

The shape of melt pool for the first scanning path had the different feature from another scanning path. Its shape was not in the tear drop style expected by Rosenthal's solution for the moving heat source. This was due to the melting and solidification of powder at the downstream of the laser path. The solidified elements, *i.e.*, the bulk element had the much higher thermal conductivity than the powder element.

(a)   (b)
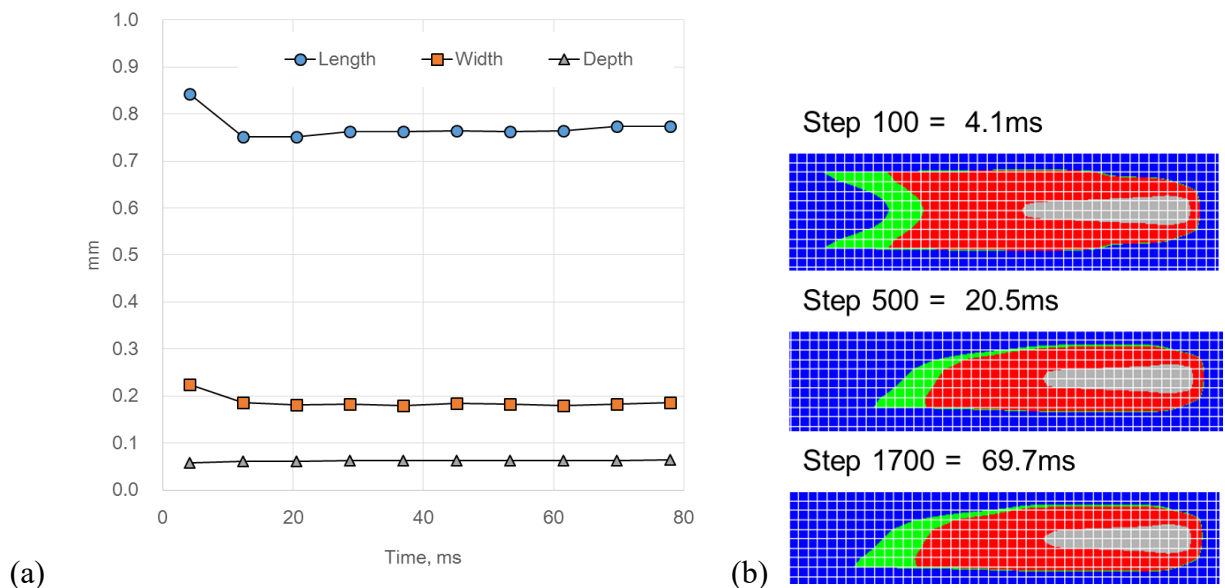
Fig. 6 Melt pool sizes with propagation of calculation (a) and melt pool profile on the top surface (b).
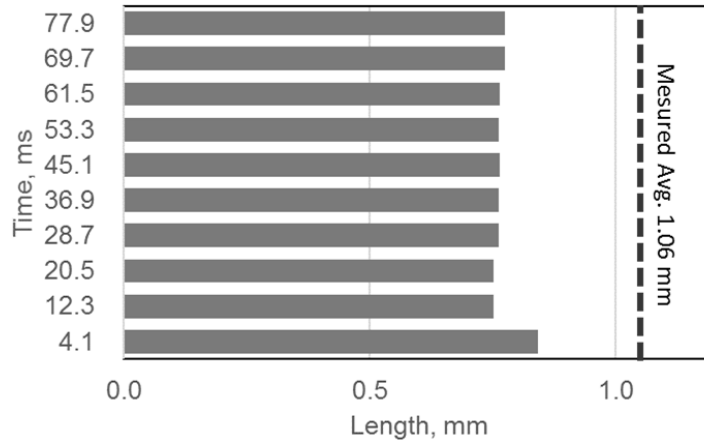
Fig.7 The estimated length of melt pool.

Discussion

The comparison of the numerically estimated melt pool length and the average value of experimentally measured melt pool length is shown in Fig.7. The numerically estimated values were approximately 70% of the experimentally obtained value. The primary reason of this underestimation might be due to the low absorption rate assumed to 0.15. In this numerical analysis, the absorption rate of 0.15 was hired due to the thermoviewer's setting on the emissivity. But, it is said that the metal powder's absorption rate is higher than its bulk surface's value. For Inconel 718, its bulk surface's absorption rate is approximately 0.2 --- 0.3. The its powder's absorption rate value might be higher than 0.3. If the absorption rate of 0.3 is used, the laser input power will be doubled and its melt pool shape might be bigger than this numerical analysis' result. But, the peak temperature of the melt pool will exceed the boiling point, and it might lead to the physically unreasonable shape of melt pool.

Another effect according to the laser input might be the how to apply the heat value as the boundary conditions. In this numerical analysis, the heat by laser was applied as heat flux on the top surface of the calculated region. Some research pointed out that the laser will infiltrated into the powder layer and it heat up the powder from its inside. So, the heat input is better to apply as the heat generation in the powder layer. And also for the solidified surface and the liquid metal, the heat input by the laser should be applied in the heat generation form. If the laser heat input is applied as the heat generation in the finite elements below the surface, the heat will be easily transferred to the subsurface of those heat generated finite elements. It will lead to the deeper melt pool shape. The heat transferred to the subsurface of the powder layer will transferred more rapidly than in the powder layer, and pre-heat the powder layer region which is not yet directly

ablated by laser from the lower side. This might enlarge the melt pool size.

Conclusion

For the selective laser melting process of Inconel 718, temperature distribution around the melt pool was measured by thermoviewer, and the length of melt pool was obtained experimentally. Transient heat transfer analysis including the melting of powder and solidification was conducted and the melt pool shape was obtained numerically. Melt pool shape of 1st path was not tear drop shape. But for 2nd path and after, it became tear drop shape. The shape of melt pool was stabilized after 4th path.

Acknowledgement

Reference

1. Wilthan B, Schuetzenhoefer W, Pottlacher G. "Thermal Diffusivity and Thermal Conductivity of Five Different Steel Alloys in the Solid and Liquid Phases". Int J Thermophys,36,8(2015)2259-72.
2. Pottlacher G, Hosaeus H, Kaschnitz E, Seifter A. "Thermophysical Properties of Solid and Liquid Inconel 718 Alloy". Scandinavian Journal of Metallurgy,31,3(2002)161-8.
3. Kunii D, "Heat Transmission of Solid Particles," Transaction of JSME, 60,456 (1957) 54-61.
4. Denlinger, E R, Jagdale, V, Srinivasan, G V, El-Wardany, T, Michaleris, P, "Thermal modeling of Inconel 718 processed with powder bed fusion and experimental validation using in situ measurements." Additive Manufacturing 11(2016)7-15.